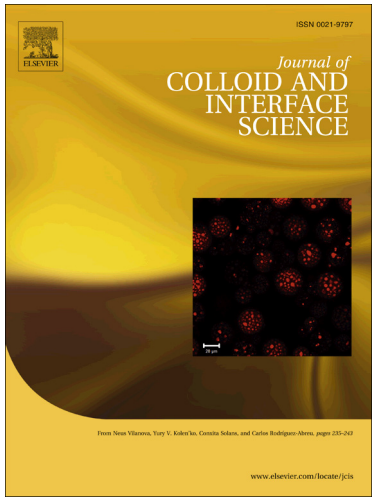

Enhanced Photocatalytic Degradation of Dyes over Graphene/Pd/TiO_2 Nanocomposites: TiO_2 Nanowires versus TiO_2 Nanoparticles

Hamed Safajou, Hossein Khojasteh, Masoud Salavati-Niasari, Sobhan Mortazavi-Derazkola

PII: S0021-9797(17)30344-2
DOI: http://dx.doi.org/10.1016/j.jcis.2017.03.078
Reference: YJCIS 22175

To appear in: *Journal of Colloid and Interface Science*

Received Date: 11 February 2017
Revised Date: 15 March 2017
Accepted Date: 18 March 2017

Please cite this article as: H. Safajou, H. Khojasteh, M. Salavati-Niasari, S. Mortazavi-Derazkola, Enhanced Photocatalytic Degradation of Dyes over Graphene/Pd/TiO_2 Nanocomposites: TiO_2 Nanowires versus TiO_2 Nanoparticles, *Journal of Colloid and Interface Science* (2017), doi: http://dx.doi.org/10.1016/j.jcis.2017.03.078

Enhanced Photocatalytic Degradation of Dyes over Graphene/Pd/TiO_2 Nanocomposites: TiO_2 Nanowires versus TiO_2 Nanoparticles

Hamed Safajou, Hossein Khojasteh, Masoud Salavati-Niasari*, Sobhan Mortazavi-Derazkola

Institute of Nano Science and Nano Technology, University of Kashan, Kashan, P. O. Box 87317–51167, Islamic Republic of Iran

**Corresponding author. Tel. +98 315 5912383; Fax +98 315 5913201*

E-mail address: salavati@kashanu.ac.ir

Abstract

In this study, at first, TiO_2 nanowire was prepared by an alkaline hydrothermal process. In the following, Gr/Pd/TiO_2-NPs and Gr/Pd/TiO_2-NWs were synthesized by a combination of hydrothermal and photodeposition methods. The properties of as prepared products were characterized using XRD, FT-IR, SEM, DRS, TEM, ICP-OES, EDS and TGA analysis. SEM results confirmed nanodimantion structure for all samples. Also the band gap values obtained using DRS technique suggests that all the samples have semiconductor behavior. Using TGA analysis, the amount of graphene loaded onto the powders was confirmed. Photocatalytic degradation of rhodamine B by TiO_2-NWs, Gr/Pd/TiO_2-NPs and Gr/Pd/TiO_2-NWs nanocomposites was compared under ultraviolet light irradiation. Results confirmed that the Gr/Pd/TiO_2-NWs composite show the highest photocatalytic activity due to much higher available surface area of TiO_2 substrate in nanowire structure. It is expected that the synthesis of the high surface area TiO_2 nanowires, facile photodeposition of palladium into its texture, and simple conversion of GO to graphene during hydrothermal process without using strong reducing agents, could be a suitable rote for preparing different types of carbon based TiO_2 nanocomposite photocatalysts.

Keywords: Graphene; Palladium; TiO_2; Nanostructures; Photocatalysis.

1. Introduction

Increasing environmental pollutions caused by heavy metals, pesticides, organic wastes and dyes in rivers and seas have provided the serious motivation to starting fundamental and applied research related to the area of environmental protection [1]. Recently, great interest has been focused on semiconductor photocatalysis using solar energy to photodegradation of water pollutants [2-4]. The applications of some semiconductors such as TiO_2 and ZnO in the area of photocatalysis have grown considerably, because they have direct wide band gap that can split photoinduced electron and holes [5]. Of the metal oxide semiconductor photocatalysts, TiO_2 has received specific attention in the field of photocatalysis and solar energy conservation due to its compatibility with other materials, inexpensive, performance stability, non-toxicity, chemical inertness, strong photo-oxidizing power, very good stability over a wide range of pH, and environmentally-friendly nature [6-8]. Titanium dioxide as a heterogeneous photocatalyst has been widely studied during the past decades and has emerged as an appropriate material for the degradation of organic pollutants to produce less toxic substances [9-11].

However, TiO_2 has the energy band gap of about 3.2 eV that makes it active only in the ultraviolet (UV) range [12]. During the past decades, much effort has been devoted to overcoming this problem and activating TiO_2 in large absorption area in the UV-vis spectra [7, 13, 14]. More photon absorption by TiO_2 leads to generate more excited charges and its activity will rise finally. One of the methods to stimulate TiO_2 under visible light is by incorporating transition metal ions into the TiO_2 context with different proportions. This action wills enhance photocatalytic activity and leads to red shift absorption edge of TiO_2 [15, 16]. Noble metals such as Ag, Au and Pt deposited on a TiO_2 surface will increase its photocatalytic activity, because they act as an electron trapping sites promoting interfacial charge transfer processes in the composites [17, 18]. Among various noble metals, palladium is a noble metal with a high catalytic activity and stability that has many technological and practical applications. For various organic reactions, the homogeneous Pd catalyst

is one of the most efficient catalytic systems that have some advantages such as fast reaction rates, excellent production yields, high turnover frequency and good selectivity [19]. Palladium often exhibits very interesting and charismatic chemical, optical, electronic and catalytic properties [20]. Also palladium is one of the most active elements for interacting with the surface of various oxides as supports. Previous researches proved that the photocatalytic performance of Pd/TiO_2 powder directly depends on the Pd crystal size and its morphology. These composite catalysts with highly dispersed small palladium nanoparticles have shown to be more active in about the strong metal-support interaction (SMSI) [21, 22]. Palladium can be used as electron acceptors to detach the photo-induced hole/electron pair and promote interfacial charge-transfer processes [23].

On the other hand, graphene has attracted special attention because of its unique structural and electronic characteristics [24]. Graphene is making when flat monolayers of carbon atoms are tightly pack into a two-dimensional (2D) honeycomb lattice. This structure can be considered as a fundamental building block for graphitic materials of all other important allotropes [25]. Even since graphene is the world's thinnest, strongest and stiffest material with light weight, as well as being an excellent conductor of heat and electricity. When graphite is oxidized to separate the carbon layers using oxygen atoms and oxygen containing functional groups, an oxidized form of graphene that is called graphene oxide (GO) will be provided [26]. Graphene oxide is an appropriate source to convert to graphene. GO is of great interest due to its low cost, easy access, scalability, non-toxic and widespread ability [27]. Particularly, graphene is highly desirable for use as a 2-D catalyst support, due to the large surface area (about 2630 m^2g^{-1}) and tunable surface properties. The surface functional groups (by modifying the surface) upon the modified graphene or graphene oxide can act as favorable sites for aggregation and nucleation of the guest materials [28]. Solution-based chemical reduction of GO have been reported as most popular procedure for the preparation of reduced GO. Previously, it has been proved that reduced GO as a conducting support can absorb catalyst nanostructures and exhibit promoted catalytic performance in different catalytic reactions [29-32].

In the present search, we accumulated and combined all the advantages of materials that mentioned above. Here we report hydrothermal and photodeposition methods that embeds Pd nanoparticles and graphene sheets into TiO_2 photocatalyst homogeneously without any functionalizing the surface or using a surfactant. Pd nanoclusters act as a sink to gather the photogenerated electrons and reducing the rate of their recombination with holes. In result, palladium impurity leads to enhance photocatalytic activity of composite [33]. On the other hand, graphene by increasing catalytic surface area, acting as efficient capping and protection of catalyst species, high adsorb ability and excellent conductivity helps to improve the separation and transportation of the charge carriers or electrons [34]. Also, another aim of this study was to make a comparison between Gr/Pd/TiO_2-NW nanocomposites in photocatalytic performance over the Gr/Pd/TiO_2-NP.

2. Experimental

2.1. Materials and characterization methods

In this work, graphite, sodium nitrate, nitric acid (65%), hydrogen peroxide (30%), sulphuric acid (98%), palladium(II) nitrate, hydrochloric acid, potassium hydroxide and methanol were purchased from Merck Company. Commercial titanium dioxide nanoparticles (P-25, 21-nm size) were purchased from Degussa Korea (Incheon, Korea). Potassium permanganate and ethanol were kindly provided by Ghatran Shimi Co (Tehran, Iran). All materials and solvents were used without further purification. Deionized water was used throughout. The products were characterized using various analytical methods. XRD patterns were recorded by a Philips, X-ray diffractometer using Ni-filtered Cu Kα radiation. The morphology and size of products were measured using scanning electron microscope, LEO instrument model 1455VP. Prior to taking images, the samples were coated with a very thin layer of Pt to make the sample surface conducting and prevent charge accumulation. GC-2550TG (Teif Gostar Faraz Company, Iran) were used for all chemical analyses. FT Infrared (FT-IR) spectra were obtained as potassium bromide pellets in the range of 400–4000 cm^{-1} with a Nicolet-Impact 400D spectrophotometer. Transmission electron microscope (TEM) images of nanopowders

were taken by a JEM-2100 with an accelerating voltage of 100 kV equipped with a high resolution CCD Camera. Thermogravimetric analysis was carried out on a Mettler TG50 instrument under air flow at a uniform heating rate of 5 °C.min^{-1} in the range 25–800 °C. The UV-Vis spectra of the samples were taken on a UV-Vis spectrophotometer (Shimadzu, UV-2550, Japan) with a 400 W Osram lamp as the light source. To determining the Pd content of the final catalyst, products were measured by an inductively coupled plasma optical emission spectrometry (ICP-OES), via a Jarrell-Ash 1100 ICP analyzer.

2.2. Synthesis of TiO_2-NWs

A facile hydrothermal approach was applied to synthesize single anatase TiO_2 NWs. Typically 20 ml solution of 10 M KOH aqueous solution was prepared followed by adding 0.5 g of TiO_2 Degussa P25 nanoparticle powders. The obtained mixture was stirred for until a homogeneous suspension was gained. After that, the obtained mixture was transferred to a 25 ml Teflon-lined autoclave (the vessel filled up to 80% of the total volume) and maintained at 190 °C for 24 h (optimized conditions). Then the autoclave was naturally cooled to room temperature and the reaction product was taken out with a forceps. To remove the residual KOH, the obtained product was successively washed with diluted HCl aqueous solution, copious amount of deionized water, and methanol for several times until the pH value was close to 7. The resulting product was recovered by centrifugation and then dried under vacuum at 60 °C to obtain white-color anatase TiO_2 NW powder.

2.3. Synthesis of Graphene oxide (GO)

GO was synthesized from graphite powder using Hummer's method [35] but with some modifications [36]. In a typical reaction, first 2 g of pristine graphite fine powder and 2 g of sodium nitrate were mixed together followed by the addition of 100 ml of concentrated sulfuric acid under constant stirring and stirring was continued for 3 hours. After that, the reaction vessel was placed in ice bath and 10 g of potassium permanganate was added gradually to the mixture. In this step the temperature should be less than 20 °C to

prevent overheating and explosion. Stirring was continued for 2 h at this temperature. The reaction mixture was subsequently transferred to a pre-heated oil bath and stirred at 35 °C for 12 h. The obtained mixture was diluted by adding 200 ml of deionized water under vigorous stirring for another 2 h.

The obtained mixture was heated to 98 °C and continuously stirred for another 12 h and then was cooled to room temperature. The suspension was further treated with 30% hydrogen peroxide solution (35 ml) to ensure the completion of reaction with $KMnO_4$. After 1 hour stirring, the final mixture was filtrated and washed with copiously amount of deionized water to completely remove the residual salts and acids followed by filtration and drying at 60 °C overnight.

2.4. Synthesis of Pd/TiO_2-NWs and Pd/TiO_2-NPs

Pd/TiO_2 nanocomposite was synthesized by photodeposition method with the ratio of 1 wt% of palladium. In this research we tried to dope both the Pd and Gr with 1w% into the catalysts because in the previous investigations we understood that this is the optimum amount for Pd and the photocatalytic performance decrease by adding excess amount of Pd [22]. For that, $Pd(NO_3)_2.2H_2O$ (0.0075 g) dissolved in 40 ml deionized water and then 0.2 gr TiO_2-NWs or TiO_2-NPs was added to synthesis of Pd/TiO_2-NWs and Pd/TiO_2-NPs respectively. The mixture was sonicated for 20 min to obtain homogeneous suspension. Then mixture was conveyed to 100 ml quartz tube and then 0.7 ml methanol added. To remove dissolved oxygen in the solution, tube contents were degased by bubbling nitrogen gas into the suspension at room temperature for 20 min. After that, the obtained suspension was stirred under UV irradiation for 10 h. At this step, palladium ions were reduced to metallic palladium and deposited on TiO_2 surface. This phenomenon can be approved by change in color of TiO_2 from white to gray. As synthesized solids were separated by centrifuging and washed with ethanol and water three times and dried at 60 ^oC for 10 h. In this process Pd was selectively deposited on the electron trapping sites. This is the key to Pd being highly deposited on TiO_2 substrate in the palladium (0) oxidation state.

2.5. Graphene/Pd/TiO_2 Nanocomposites

To synthesize graphene/Pd/TiO_2 nanocomposites, hydrothermal method was employed. In the beginning, 2 mg of GO was added into a solution of 40 ml of deionized water and 15 ml of methanol. The mixture was stirred in ultrasonic bath for 30 min to re-exfoliate the GO thoroughly. In the next step, 0.2 g of TiO_2 nanowires or TiO_2 nanoparticles that was prepared in 2.4 section were added to the GO suspension to synthesis of Gr/Pd/TiO_2-NWs and Gr/Pd/TiO_2-NPs respectively. Then the sonication and stirring was employed alternately for 1 h with 20 min for each mixture until a homogeneous suspension was achieved, which shows a uniform light gray color. The as prepared suspensions was then transferred into a Teflon-lined autoclave again and maintained at 140 °C for 5 h to synthesize the graphene/Pd/TiO_2 nanocomposites. During this process, reduction of GO was also realized with methanol as the active reductant agent. After being cooled down to ambient temperature, the ultimate suspension was centrifuged at 7000 rpm for 5 min, washed with deionized water several times and dried at ambient condition.

2.6. Photocatalytic measurements

The process of degradation of rhodamine B as a water pollutant was studied to investigate the catalytic activity of as prepared photocatalysts. The photocatalytic performance of the Gr/Pd/TiO_2-NWs and Gr/Pd/TiO_2-NPs catalysts was investigated using a 100 ml quartz tube. Typically 0.03 g of each photocatalyst was mixed with 40 ml of rhodamine B solution with initial concentration of about 10 ppm. As we know, protonation of rhodamine B that enriched the hydrophobicity of the molecules lead to improvement in the degradation efficiency of dye in acidic medium. Also, H_2O_2 molecules that were formed during UV irradiation could become very unstable in basic environment, so to intense rhodamine B photodegradation rate, finally 1 ml of HNO_3 65% added to vessels. In the following, to obtain the maximum absorption of organic pollutant molecules on the photocatalyst surface, to make oxygen available for the reaction and to obtain most homogeneity in the mixture, stirring was continued with bubbling air into suspensions. The photodegradation

reaction was carried out under the UV light irradiation and the mixtures were placed inside the photoreactors in which the vessels were 40 cm away from the UV source of 400 W Mercury lamp. After each 10 or 15 min period, the sample was centrifuged to measure the absorbance using the UV–Vis spectrometer.

3. Results and discussion

The as synthesized products were characterized using XRD, FT-IR, SEM, TEM, ICP(OES), EDS, DRS & TGA analysis.

3.1. XRD characterization

The obtained powder XRD patterns for TiO_2 P25, Pd/TiO_2-NWs and Gr/Pd/TiO_2-NWs are shown in Fig.1. As shown, the TiO_2-NWs displayed a similar XRD pattern to the pure TiO_2 P25 nanopowders with the typical diffraction peak of anatase phase and rutile peaks. The emerged peaks at 2θ= 25.6, 38.17, 48.32, 54.36, 55.4, 63.02, 69.15, 70.59 and 75.33 is consistent with the values on the JCPDS card (no: 04-0477) which show the anatase-phase for TiO_2. In addition, the XRD pattern of Gr/Pd/TiO_2-NWs was also similar to previous patterns. This observation suggests that the hydrothermal and photodeposition methods to preparing of the composites synthesis have no obvious impress on the original TiO_2 crystallization. Furthermore, as seen, the original rutile peaks in TiO_2 P25 NPs were vanished for Pd/TiO_2-NWs and Gr/Pd/TiO_2-NWs samples. This result indicates that the small fraction of rutile phase in P25 NPs has almost disappeared or transformed to anatase phase during preparation process [37]. Also, because of small amount and weak intensity of graphene and palladium impurity, no diffraction peaks associates to carbon or palladium species have been observed (Fig.1c).

3.2. FT-IR analysis

Here FT-IR technique was used to study the bonding interactions in the synthesized materials. Fig.2 shows the FT-IR spectrum for TiO_2-NWs, Gr/Pd/TiO_2-NPs and Gr/Pd/TiO_2-NWs. For TiO_2-NW and Gr/Pd/TiO_2-

NP, broad band at about 3440 cm^{-1} was assigned to the stretching vibrations of surface hydroxyl (-OH) groups. Due to large amount of hydroxyl functional groups, this peak has high intensity in TiO_2-NWs and Gr/Pd/TiO_2-NWs samples. In addition, all samples showed low frequency bands around 692 cm^{-1}, which were assigned to the stretching of Ti–O bond and bending of O–Ti–O bond. For Gr/Pd/TiO_2-NPs, a broad band at approximately 500 cm^{-1} can be seen which is attributed to different vibrational modes of rutile phases of TiO_2 in Gr/Pd/TiO_2-NPs structure as described in XRD characterization. The absorption signal at about 790 cm^{-1} was attributed to the formation of Ti–O–C bonds which confirms that the chemical bonds were firmly built between graphene and TiO_2 nanostructures [38]. Both synthesized Gr/Pd/TiO_2-NPs and Gr/Pd/TiO_2-NWs have absorption peaks at approximately 2925 cm^{-1} and 2850 cm^{-1} corresponding to the symmetric and anti-symmetric stretching vibrations frequency of CH_2 groups caused by graphene content. Finally, the absorption band at approximately 1640 cm^{-1} is ascribed to C=C bending vibrations of graphene.

3.3 Morphology of products

The SEM micrographs of synthesized products are given in Fig.3. From SEM image of the as-made titanate NWs (Fig.3a), it is clear that the TiO_2-NWs are abundant in quantity and pretty tidy with smooth surface and have woven together. SEM micrograph of the Gr/Pd/TiO_2-NPs composite exhibits nanoscale textures and is indicative of a much rougher surface in compare with other samples (Fig.3b). SEM results of Gr/Pd/TiO_2-NPs composite also show that the Pd/TiO_2 particle size was in nanometers. Fig.3c shows a typical SEM image of the as-prepared Gr/Pd/TiO_2-NWs. Compared with Pd/TiO_2-NPs, which are anchored on GO along its wrinkles and edges with agglomeration, the Pd/TiO_2-NWs are anchored on to the reduced GO sheets after hydrothermal treatment in a reasonably uniform fashion, with smooth surface and without agglomeration.

3.4. EDS analysis

Owing to the small amount of Pd (about 1%) in the catalyst structure, for Gr/Pd/TiO_2-NPs and Gr/Pd/TiO_2-NWs samples, no specific peak related to Pd was observed in previous analytical techniques. According to

this, to prove the presence of palladium in the structure, an elemental analysis (EDS) for Gr/Pd/TiO_2-NWs sample was taken. So to confirm the chemical composition of the synthesized powders, the sample was examined by EDS analysis (Fig.4). This spectrum confirms that the targeted chemical composition could achieve in the final product. Obviously, the sample is composed of C, O, Ti, and Pd elements. In compare with Pd, the intense signal of C is seen in the spectrum which is due to the all carbon content of graphene and also carbon film used for supporting the sample. For estimating the real amount of the palladium in the structure, Gr/Pd/TiO_2-NPs and Gr/Pd/TiO_2-NWs nanocomposites were measured by an inductively coupled plasma optical emission spectrometry and the presence of palladium in the nanocomposites was confirmed which showed a value of about 0.087 and 0.09 mmol Pd per gram of catalyst respectively.

3.5. TEM analysis

Transmission electron microscopy analysis is a powerful technique to confirming the accurately size and thickness of nanostructures. Fig.5 shows a typical transmission electron microscope (TEM) image of the as-prepared TiO_2-NWs and Gr/Pd/TiO_2-NWs composite. It can be noticed from the TEM images that the as-synthesized TiO_2-NWs have a length of several micrometers and about 50 nm (Fig.5a). Moreover, the TEM image for Gr/Pd/TiO_2-NWs composite shows that the reduced graphene oxide acts as a matrix for the titanate nanowires. It can be seen that TiO_2-NWs occupy most of the available surface area of reduced GO (Fig.5b).

3.5. Thermogravimetric characterization

Thermal properties of Gr/Pd/TiO_2-NPs and Gr/Pd/TiO_2-NWs were studied using TGA analysis and the obtained curves are shown in Fig.6. The loading of graphene into the Pd/TiO_2 nanostructures was determined through performing TGA experiment in air and heating up the sample from ambient temperature to 750 °C. Both samples display two significant weight loss events at approximately 275 and 650 °C. Small mass decrease for Gr/Pd/TiO_2-NPs sample revealed that this sample relatively is stable to thermal treatment below 800 °C under air atmosphere. For both samples, major weight loss was observed in the first step below 300 °C

(100–275) corresponding to the vaporization of adsorbed and bound water on the graphene and powder surface [39]. This weigh loss was about 1.58% for Gr/Pd/TiO_2-NPs sample (Fig.6a). TGA result reveals that Gr/Pd/TiO_2-NPs lose 1.06 % of its weight in between 300–650 °C (a total weight loss of 2.64 wt% at 650 °C), which is attributed to a loss and combustion of graphene content in air. This observation indicates that the amount of graphene loaded into the Gr/Pd/TiO_2-NPs sample was about 1.06 wt.%.

For the Gr/Pd/TiO_2-NWs large weight loss peak was observed at 150 °C, illustrating that the Pd/TiO_2-NWs absorb more water and solvent in compare with Pd/TiO_2-NPs (Fig.6b). Between 300 and 650 °C, a slower mass loss was happened that can be attributed to the destruction of the carbon skeleton of graphene [40]. Overall, Gr/Pd/TiO_2-NWs sample reached a total weight loss of 6.83 wt% at 650 °C in air atmosphere. The weight loss of Gr/Pd/TiO_2-NWs was stabilized at about 98.68% at temperatures between 300 and 650 °C, which indicate that the amount of graphene loaded into the structure, was about 1.3 wt%.

3.6. Light absorption and band gap study

The absorption coefficient and optical band gap of a material are two important parameters by which the optical characteristics. Light absorption by the material and the migration of the light-induced electrons and holes are the key factors controlling a photocatalytic reaction. These features are related to the electronic structure characteristics of the material. The absorbance of Gr/Pd/TiO_2-NPs and Gr/Pd/TiO_2-NWs nanostructures as a function of wavelength and the plot calculated by the transformation based on the Kubelka–Munk function versus the energy of samples have been illustrated in Fig. 7. As shown both the nanocomposites are photo-responsive in the UV ranges (250–350 nm) that corresponds to band-to-band transition from the Ti(3d) level of titanium (conduction band) to O(2p) level of oxygen as valence band. However, the Gr/Pd/TiO_2-NWs sample has a visible light response in the region between 360 and 430 nm and compared with Gr/Pd/TiO_2-NPs, the absorption edge is significantly extended towards the visible light range for Gr/Pd/TiO_2-NWs. This is attributed to the charge-transfer transition between the Pd^{2+} d-electrons and the

TiO_2 conduction or valence band. This observation probably relates to more available Pd species due to more surface area of TiO_2-NWs in compare with TiO_2-NPs. Final result of this observation is the increasing of the photocatalytic activity for Gr/Pd/TiO_2-NWs sample in compare with Gr/Pd/TiO_2-NPs.

3.7. Investigation of photocatalytic activity

During the photocatalysis process, the mechanism of photodegradation involves three steps including adsorption of the pollutant, absorption of inducer light by the photocatalyst, and charge transfer reactions to create radical and active species to decompose the dye or pollutants. Photocatalytic degradation of rhodamine B by TiO_2-NWs, TiO_2-NPs, Pd/TiO_2-NPs, Gr/Pd/TiO_2-NPs and Gr/Pd/TiO_2-NWs nanocomposites was performed under ultraviolet light irradiation and changes in dye concentration were followed by UV absorption spectroscopy.

The degradation of rhodamine B our time t (DP(t)) was calculated using the follows equation:

$$DP(t) = \frac{A_0 - A_t}{A_0} \times 100 \qquad (1)$$

Here, A_0 and A_t are the absorbance values of the solution at 0 and t minutes, respectively. As we know most industrial dyes and related pollutants has aromatic nature and usually create π-π stacking interactions with the aromatic domains of other aromatic materials such as graphene. This phenomenon significantly enhances the concentration of the pollutant molecules near the surface of the catalyst that is an important contributing factor for achieving higher photocatalytic degradation activities.

To confirm the catalysts effect, first the mixture stirred in dark conditions. After 40 minutes, no dye degradation was observed without using light source or photocatalysts, so the contribution of self-degradation is insignificant. To proving that the adsorption process is not significant, we made a similar experiment and the dye solution with the photocatalyst stirred in dark conditions for 60 min. The changes in dye concentration were followed by UV absorption spectroscopy. Results proved that the reduction in dye concentration is very

insignificant. According to this observation, we conclude that because just after turning on the UV light, the color of the solution changes to paler, so here Rhodamine B is decompose and not adsorbed on the composite. After turning on the UV lamp, as time passed, the dye was decomposed and the color of the solution became brighter and a rather transparent solution was obtained after 50 min reaction time as shown in Fig. 8. Results for rhodamine B decomposition were recorded in Fig. 9 and it confirmed that most dye degradation processes occur in the initial minutes of reaction. After 40 minutes, the rhodamine B degradation was obtained at 62% for TiO_2-NPs, 66% for TiO_2-NWs, 76% for Pd/TiO_2-NPs, while it was about 79% for Gr/Pd/TiO_2-NPs and 90 % for Gr/Pd/TiO_2-NWs sample. It also can be seen that the degradation rate of all samples in initial minutes is higher. Because of decrement of dye molecules surround the catalyst nanoparticles, over the time, the degradation rate was decreased. Here the palladium species acts as an electron acceptor and by collecting the photo-induced electrons lead to decrease the recombination probability of photoinduced electrons with their counterparts.

The final result of this process is increasing in fraction of photoholes available for the oxidizing interfacial charge-transfer reactions, producing active sites for dye degradation and promoting dye decomposition. On the other hand, since graphene is a zero-band-gap semiconductor owing to its two-dimensional (2D) plate-like structure, thus has a high electrical conductivity in storing and shuttling electrons. So the combination of these advantages allows to photocatalyst showcasing high catalytic performance. To further understand the photodegradation process, a proposed photocatalytic mechanism in the presence of Pd NPs and graphene, is depicted in Fig. 10.

As we know, for practical application, the stability for the catalyst is quite important. So the cyclic experiment was investigated for Gr/Pd/TiO_2-NWs sample. The catalyst recycling was carried out in the same previous reaction condition as described in 2.6 sections. After each 50 minutes, the catalyst was collected by centrifuging and washed by water and acetone, successively. The dried powder was reused in next catalytic

cycle with fresh reactants and results were recorded in Fig. 11. As shown, the Gr/Pd/TiO_2-NWs catalyst was reused five consecutive cycles without significant reduction in catalytic performance. So the Gr/Pd/TiO_2-NWs were used as efficient heterogeneous catalysts for the dye degradation reaction under UV irradiation. Modification of the nanowire TiO_2 photocatalyst by Gr and clusters resulted in a significant effect on catalytic activity in compare with other samples.

4. Conclusion

In summary, herein we described an effective procedure to synthesize Gr/Pd/TiO_2-NPs and Gr/Pd/TiO_2-NWs photocatalysts. The method that we developed has some advantages for synthesizing novel TiO_2, graphene and palladium nanocomposites for using as photocatalysts. For example we were able to replace conventional TiO_2 nanoparticle on reduced graphene approach with high surface area nanowire TiO_2 on reduced graphene oxide to obtain more efficient photocatalyst. Typically, hydrothermally grown nanowires show much higher surface area. Also, we observed the hydrothermal conditions easily convert GO to reduced graphene oxide. In addition, after that, palladium ions were exposed with UV irradiation, the ions reduced to metallic palladium and deposited on TiO_2 surface efficiently. As prepared photocatalysts, were evaluated for dye degradation reaction. Palladium species acts as an electron acceptor by collecting the photo-induced electrons and graphene acts as high electrical conductive path for photo-generated electrons resulting to producing active sites for dye degradation and promoting dye decomposition. In contrast to Gr/Pd/TiO_2-NPs, Gr/Pd/TiO_2-NWs have much higher surface area with an enormous number of active sites leading to more efficient activity in degradation of rhodamine B. Moreover, results indicate that Gr/Pd/TiO_2-NWs photocatalyst has great potential for recycling and stability over five separation cycles.

Acknowledgment

Authors are grateful to the council of Iran National Science Foundation (INSF) and University of Kashan for supporting this work by Grant No (159271/5979).

Abbreviations

$Gr/Pd/TiO_2$-NW = $Gr/Pd/TiO_2$- Nanowire	$Gr/Pd/TiO_2$-NP = $Gr/Pd/TiO_2$-Nanoparticle
Gr = Graphene	GO = Graphene oxide
TNBT = Tetranormalbuthyltitanate	SEM = Scanning electron microscope
EDS = energy dispersive X-ray spectroscopy	TGA = Thermogravimetric analysis
DRS= Diffuse reflectance spectroscopy	ICP-OES= Inductively coupled plasma optical emission spectrometry

References

[1] H. Kyung, J. Lee, W. Choi, Simultaneous and Synergistic Conversion of Dyes and Heavy Metal Ions in Aqueous TiO2 Suspensions under Visible-Light Illumination, Environmental Science & Technology 39(7) (2005) 2376-2382.

[2] J. Guo, S. Zhu, Z. Chen, Y. Li, Z. Yu, Q. Liu, J. Li, C. Feng, D. Zhang, Sonochemical synthesis of TiO2 nanoparticles on graphene for use as photocatalyst, Ultrasonics Sonochemistry 18(5) (2011) 1082-1090.

[3] Z. Xiong, L.L. Zhang, J. Ma, X.S. Zhao, Photocatalytic degradation of dyes over graphene-gold nanocomposites under visible light irradiation, Chemical Communications 46(33) (2010) 6099-6101.

[4] V.K. Vidhu, D. Philip, Catalytic degradation of organic dyes using biosynthesized silver nanoparticles, Micron 56 (2014) 54-62.

[5] Y. Min, K. Zhang, L. Chen, Y. Chen, Y. Zhang, Ionic liquid assisting synthesis of ZnO/graphene heterostructure photocatalysts with tunable photoresponse properties, Diamond and Related Materials 26 (2012) 32-38.

[6] H.-i. Kim, G.-h. Moon, D. Monllor-Satoca, Y. Park, W. Choi, Solar Photoconversion Using Graphene/TiO2 Composites: Nanographene Shell on TiO2 Core versus TiO2 Nanoparticles on Graphene Sheet, The Journal of Physical Chemistry C 116(1) (2012) 1535-1543.

[7] H. Khojasteh, M. Salavati-Niasari, S. Mortazavi-Derazkola, Synthesis, characterization and photocatalytic properties of nickel-doped TiO2 and nickel titanate nanoparticles, Journal of Materials Science: Materials in Electronics 27(4) (2016) 3599-3607.

[8] H.L. Chen, P. Luo, Z.Y. Huang, H.P. Chen, M. Chen, D.H. Chen, Preparation and blood compatibility of carbon/TiO2 nanocomposite, Diamond and Related Materials 38 (2013) 52-58.

[9] I. Oller, W. Gernjak, M.I. Maldonado, L.A. Pérez-Estrada, J.A. Sánchez-Pérez, S. Malato, Solar photocatalytic degradation of some hazardous water-soluble pesticides at pilot-plant scale, Journal of Hazardous Materials 138(3) (2006) 507-517.

[10] S. Chin, E. Park, M. Kim, J. Jurng, Photocatalytic degradation of methylene blue with TiO2 nanoparticles prepared by a thermal decomposition process, Powder Technology 201(2) (2010) 171-176.

[11] M. Ban, N. Hasegawa, Deposition of diamond-like carbon thin films containing photocatalytic titanium dioxide nanoparticles, Diamond and Related Materials 25 (2012) 92-97.

[12] K. Prabakar, T. Takahashi, T. Nezuka, K. Takahashi, T. Nakashima, Y. Kubota, A. Fujishima, Visible light-active nitrogen-doped TiO2 thin films prepared by DC magnetron sputtering used as a photocatalyst, Renewable Energy 33(2) (2008) 277-281.

[13] T. Ihara, M. Miyoshi, Y. Iriyama, O. Matsumoto, S. Sugihara, Visible-light-active titanium oxide photocatalyst realized by an oxygen-deficient structure and by nitrogen doping, Applied Catalysis B: Environmental 42(4) (2003) 403-409.

[14] S.U.M. Khan, M. Al-Shahry, W.B. Ingler, Efficient Photochemical Water Splitting by a Chemically Modified n-TiO2, Science 297(5590) (2002) 2243-2245.

[15] C.-H. Chang, Y.-H. Shen, Synthesis and characterization of chromium doped SrTiO3 photocatalyst, Materials Letters 60(1) (2006) 129-132.

[16] H. Kato, A. Kudo, Visible-Light-Response and Photocatalytic Activities of TiO2 and SrTiO3 Photocatalysts Codoped with Antimony and Chromium, The Journal of Physical Chemistry B 106(19) (2002) 5029-5034.

[17] A. Orlov, D.A. Jefferson, N. Macleod, R.M. Lambert, Photocatalytic Properties of TiO2 Modified with Gold Nanoparticles in the Degradation of 4-Chlorophenol in Aqueous Solution, Catalysis Letters 92(1) (2004) 41-47.

[18] A. Yamakata, T.-a. Ishibashi, H. Onishi, Electron- and Hole-Capture Reactions on Pt/TiO2 Photocatalyst Exposed to Methanol Vapor Studied with Time-Resolved Infrared Absorption Spectroscopy, The Journal of Physical Chemistry B 106(35) (2002) 9122-9125.

[19] Y. Bai, L.M.H. Kim, H. Liao, X.-W. Liu, Oxidative Heck Reaction of Glycals and Aryl Hydrazines: A Palladium-Catalyzed C-Glycosylation, The Journal of Organic Chemistry 78(17) (2013) 8821-8825.

[20] M.C. Roco, Broader Societal Issues of Nanotechnology, Journal of Nanoparticle Research 5(3) (2003) 181-189.

[21] J. Panpranot, K. Kontapakdee, P. Praserthdam, Selective hydrogenation of acetylene in excess ethylene on micron-sized and nanocrystalline TiO2 supported Pd catalysts, Applied Catalysis A: General 314(1) (2006) 128-133.

[22] H. Khojasteh, M. Salavati-Niasari, A. Abbasi, F. Azizi, M. Enhessari, Synthesis, characterization and photocatalytic activity of PdO/TiO2 and Pd/TiO2 nanocomposites, Journal of Materials Science: Materials in Electronics 27(2) (2016) 1261-1269.

[23] G. Strukul, R. Gavagnin, F. Pinna, E. Modaferri, S. Perathoner, G. Centi, M. Marella, M. Tomaselli, Use of palladium based catalysts in the hydrogenation of nitrates in drinking water: from powders to membranes, Catalysis Today 55(1–2) (2000) 139-149.

[24] C.N.R. Rao, A.K. Sood, K.S. Subrahmanyam, A. Govindaraj, Graphene: The New Two-Dimensional Nanomaterial, Angewandte Chemie International Edition 48(42) (2009) 7752-7777.

[25] A.K. Geim, K.S. Novoselov, The rise of graphene, Nat Mater 6(3) (2007) 183-191.

[26] L. Sun, B. Fugetsu, Mass production of graphene oxide from expanded graphite, Materials Letters 109 (2013) 207-210.

[27] P.B. Arthi G, L. Bd, A Simple Approach to Stepwise Synthesis of Graphene Oxide Nanomaterial, Journal of Nanomedicine & Nanotechnology 06(01) (2015).

[28] P.V. Kamat, Graphene-Based Nanoarchitectures. Anchoring Semiconductor and Metal Nanoparticles on a Two-Dimensional Carbon Support, The Journal of Physical Chemistry Letters 1(2) (2010) 520-527.

[29] L. David, R. Bhandavat, G. Kulkarni, S. Pahwa, Z. Zhong, G. Singh, Synthesis of Graphene Films by Rapid Heating and Quenching at Ambient Pressures and Their Electrochemical Characterization, ACS Applied Materials & Interfaces 5(3) (2013) 546-552.

[30] K. Jasuja, J. Linn, S. Melton, V. Berry, Microwave-Reduced Uncapped Metal Nanoparticles on Graphene: Tuning Catalytic, Electrical, and Raman Properties, The Journal of Physical Chemistry Letters 1(12) (2010) 1853-1860.

[31] Z. Li, J. Liu, Z. Huang, Y. Yang, C. Xia, F. Li, One-Pot Synthesis of Pd Nanoparticle Catalysts Supported on N-Doped Carbon and Application in the Domino Carbonylation, ACS Catalysis 3(5) (2013) 839-845.

[32] F. Meng, J. Li, S.K. Cushing, M. Zhi, N. Wu, Solar Hydrogen Generation by Nanoscale p–n Junction of p-type Molybdenum Disulfide/n-type Nitrogen-Doped Reduced Graphene Oxide, Journal of the American Chemical Society 135(28) (2013) 10286-10289.

[33] H. Khojasteh, M. Salavati-Niasari, M.-P. Mazhari, M. Hamadanian, Preparation and characterization of Fe3O4@SiO2@TiO2@Pd and Fe3O4@SiO2@TiO2@Pd-Ag nanocomposites and their utilization in enhanced degradation systems and rapid magnetic separation, RSC Advances 6(81) (2016) 78043-78052.

[34] R. Huang, H. Ge, X. Lin, Y. Guo, R. Yuan, X. Fu, Z. Li, Facile one-pot preparation of [small alpha]-SnWO4/reduced graphene oxide (RGO) nanocomposite with improved visible light photocatalytic activity and anode performance for Li-ion batteries, RSC Advances 3(4) (2013) 1235-1242.

[35] W.S. Hummers Jr, R.E. Offeman, Preparation of graphitic oxide, Journal of the American Chemical Society 80(6) (1958) 1339-1339.

[36] D.N.H. Tran, S. Kabiri, D. Losic, A green approach for the reduction of graphene oxide nanosheets using non-aromatic amino acids, Carbon 76 (2014) 193-202.

[37] X. Pan, Y. Zhao, S. Liu, C.L. Korzeniewski, S. Wang, Z. Fan, Comparing Graphene-TiO2 Nanowire and Graphene-TiO2 Nanoparticle Composite Photocatalysts, ACS Applied Materials & Interfaces 4(8) (2012) 3944-3950.

[38] H. Zhang, X. Lv, Y. Li, Y. Wang, J. Li, P25-Graphene Composite as a High Performance Photocatalyst, ACS Nano 4(1) (2010) 380-386.

[39] S. Stankovich, D.A. Dikin, R.D. Piner, K.A. Kohlhaas, A. Kleinhammes, Y. Jia, Y. Wu, S.T. Nguyen, R.S. Ruoff, Synthesis of graphene-based nanosheets via chemical reduction of exfoliated graphite oxide, Carbon 45(7) (2007) 1558-1565.

[40] J. Guo, Y. Li, S. Zhu, Z. Chen, Q. Liu, D. Zhang, W.-J. Moon, D.-M. Song, Synthesis of WO3@Graphene composite for enhanced photocatalytic oxygen evolution from water, RSC Advances 2(4) (2012) 1356-1363.

Figure captions

Fig.1. XRD patterns for TiO_2 P25, Pd/TiO_2-NWs and Gr/Pd/TiO_2-NWs nanostructures.

Fig.2. FT-IR spectrum for TiO_2-NWs, Gr/Pd/TiO_2-NPs and Gr/Pd/TiO_2-NWs.

Fig.3. SEM images of a) TiO_2-NWs, b) Gr/Pd/TiO_2-NPs and c) Gr/Pd/TiO_2-NWs nanocomposites.

Fig.4. EDS for Gr/Pd/TiO_2-NWs nanocomposite.

Fig.5. TEM images of the TiO_2 nanowires (a) and Gr/Pd/TiO_2-NWs nanostructures (b).

Fig.6. TGA curve of a) Gr/Pd/TiO_2-NPs and b) Gr/Pd/TiO_2-NWs

Fig.7. UV–Vis spectrum (DRS) and calculated band gap for Gr/Pd/TiO_2-NPs and Gr/Pd/TiO_2-NWs nanocomposites.

Fig.8. Rhodamine B after 50 minutes photodegradation in the presence of Gr/Pd/TiO_2-NWs nanocomposite.

Fig.9. Plot of percentage degradation Vs time for photocatalytic dye degradation.

Fig.10. Mechanism of catalyst performance.

Fig. 11. Recycling experiment for Gr/Pd/TiO_2-NWs nanocatalyst.

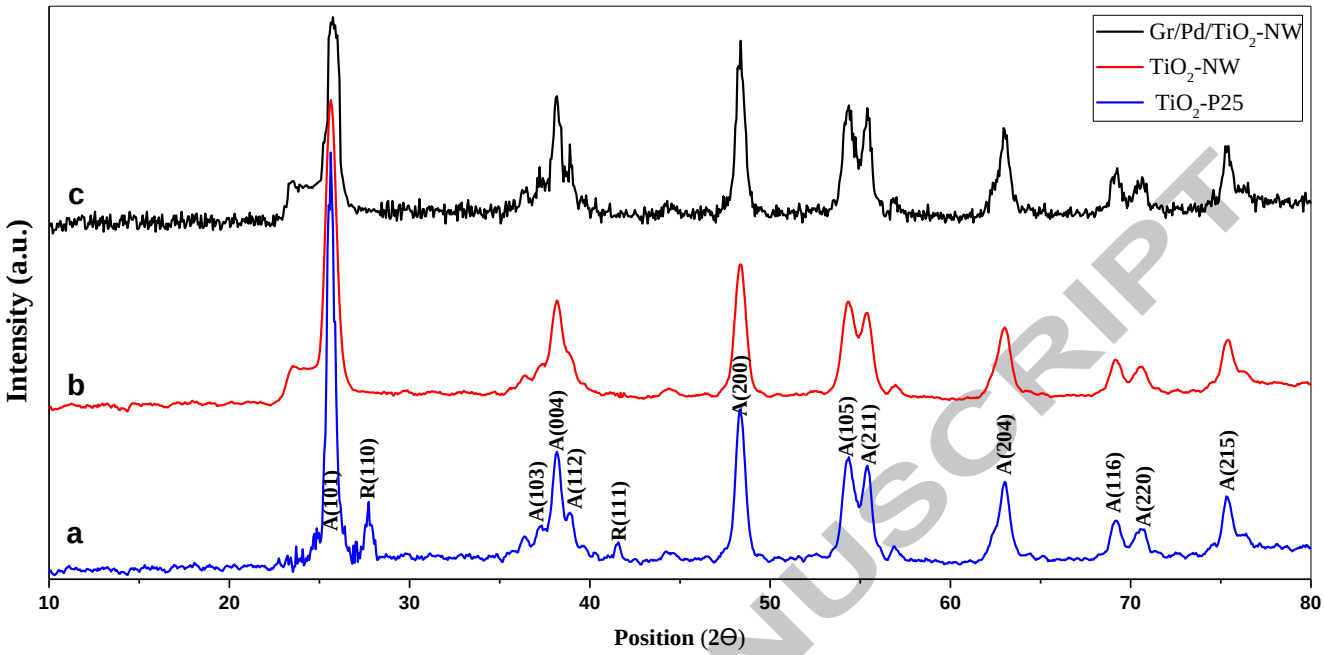

Fig.1.

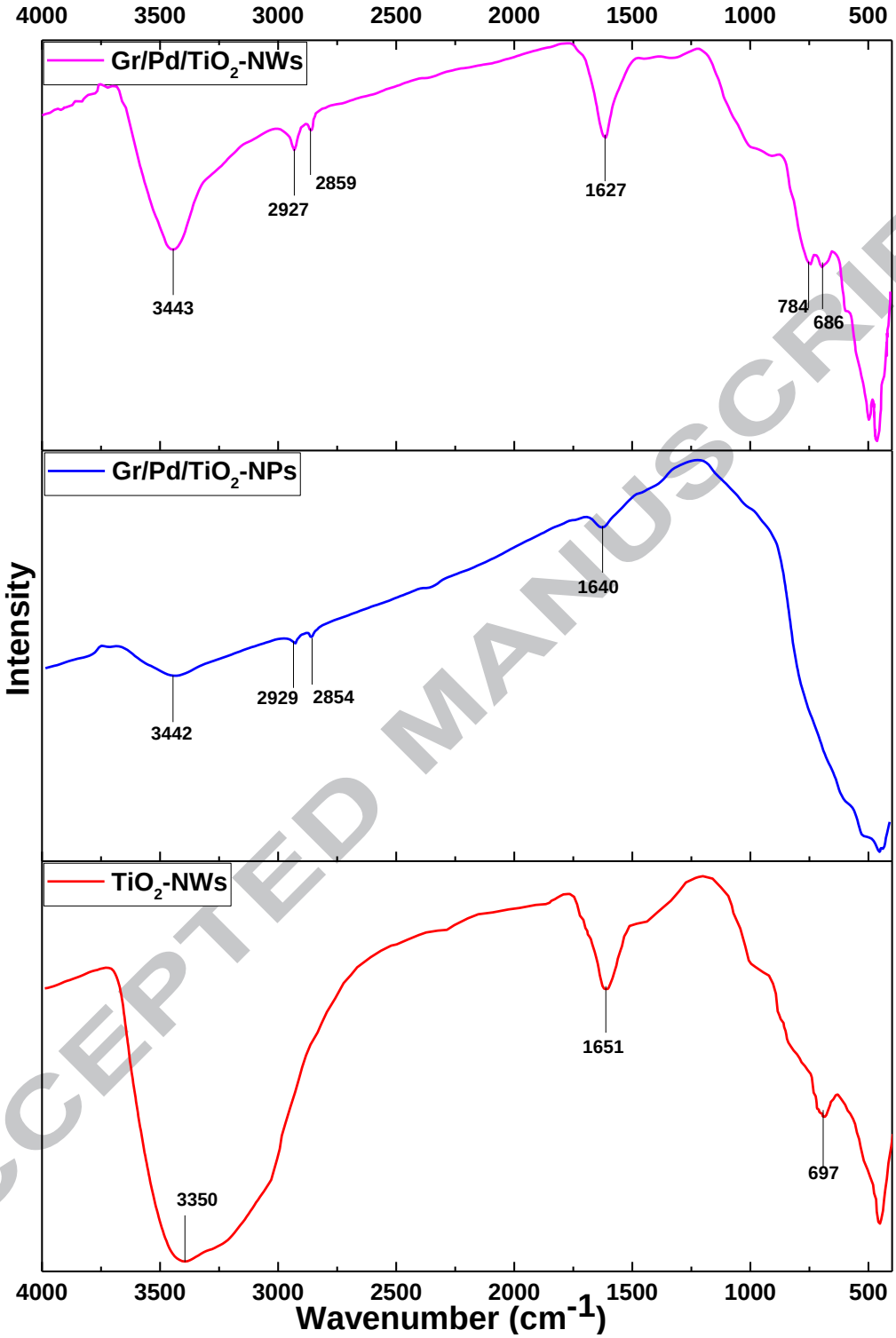

Fig.2.

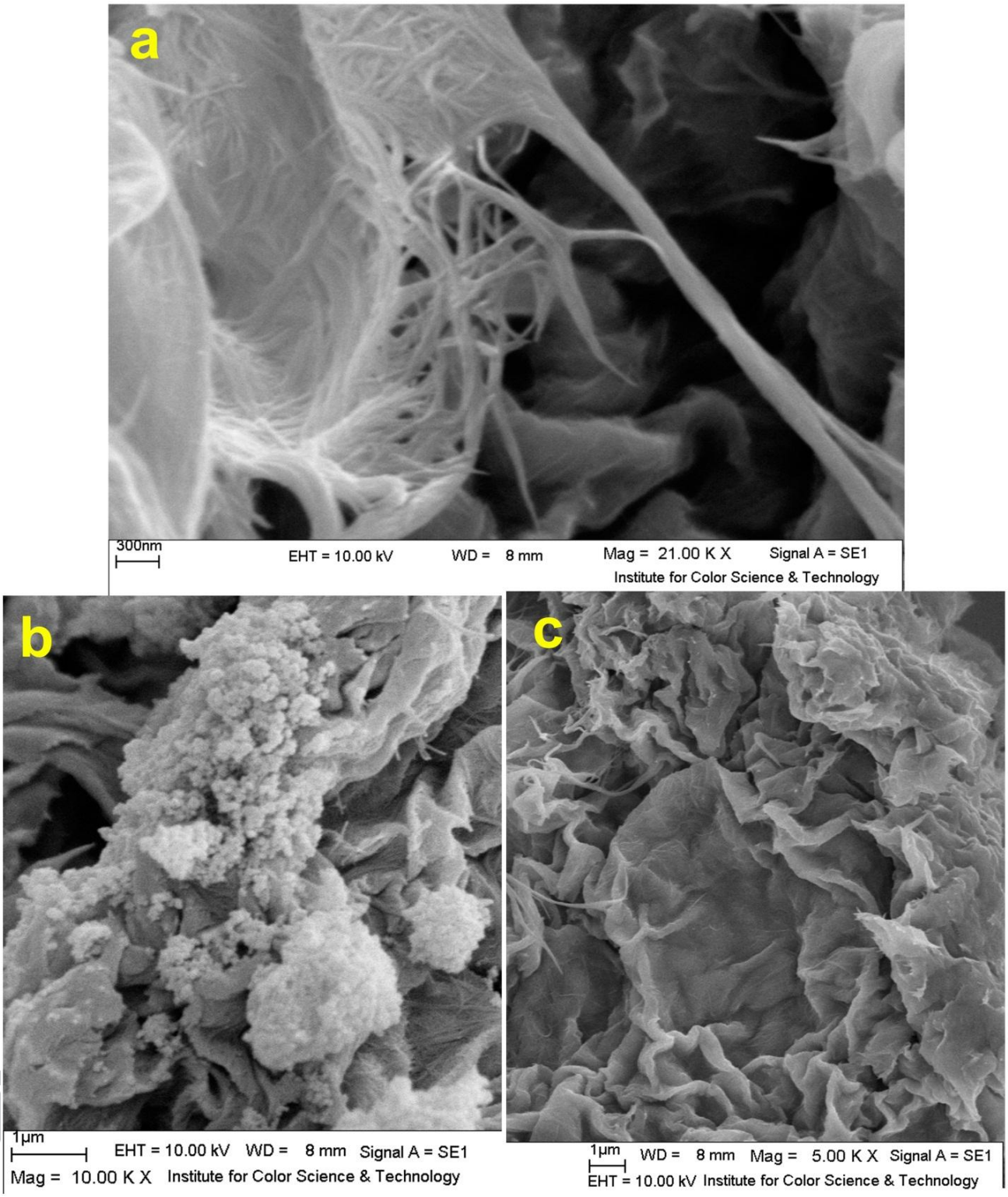
a
300nm
EHT = 10.00 kV
WD = 8 mm
Mag = 21.00 K X
Signal A = SE1
Institute for Color Science & Technology
b
1µm
EHT = 10.00 kV
WD = 8 mm
Signal A = SE1
Mag = 10.00 K X
Institute for Color Science & Technology
c
1µm
WD = 8 mm
Mag = 5.00 K X
Signal A = SE1
EHT = 10.00 kV
Institute for Color Science & Technology

Fig.3.

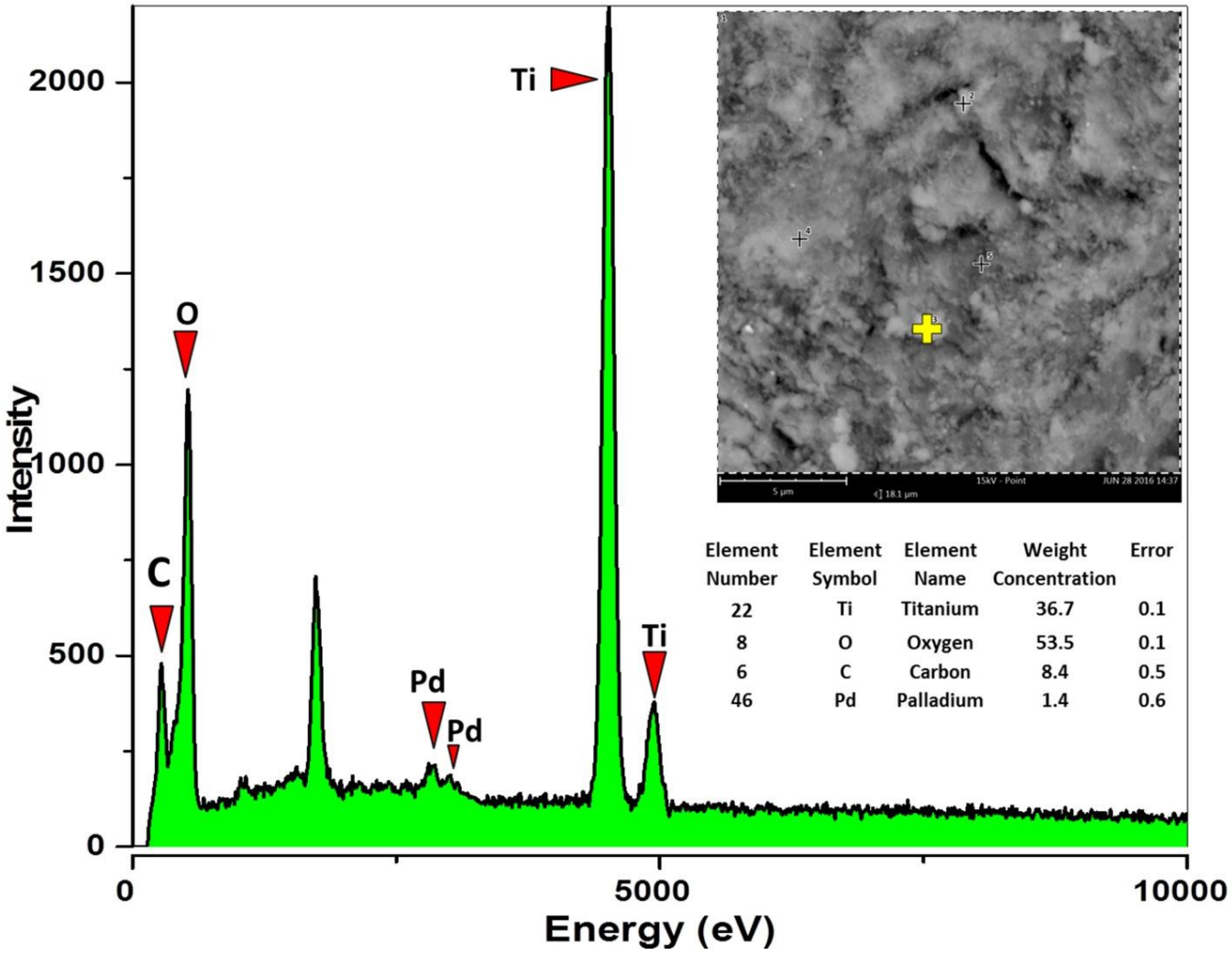
Intensity
Energy (eV)
0
500
1000
1500
2000
0
5000
10000
C
O
Pd
Pd
Ti
Ti
Element Number
Element Symbol
Element Name
Weight Concentration
Error
22 Ti Titanium 36.7 0.1
8 O Oxygen 53.5 0.1
6 C Carbon 8.4 0.5
46 Pd Palladium 1.4 0.6

Fig.4.

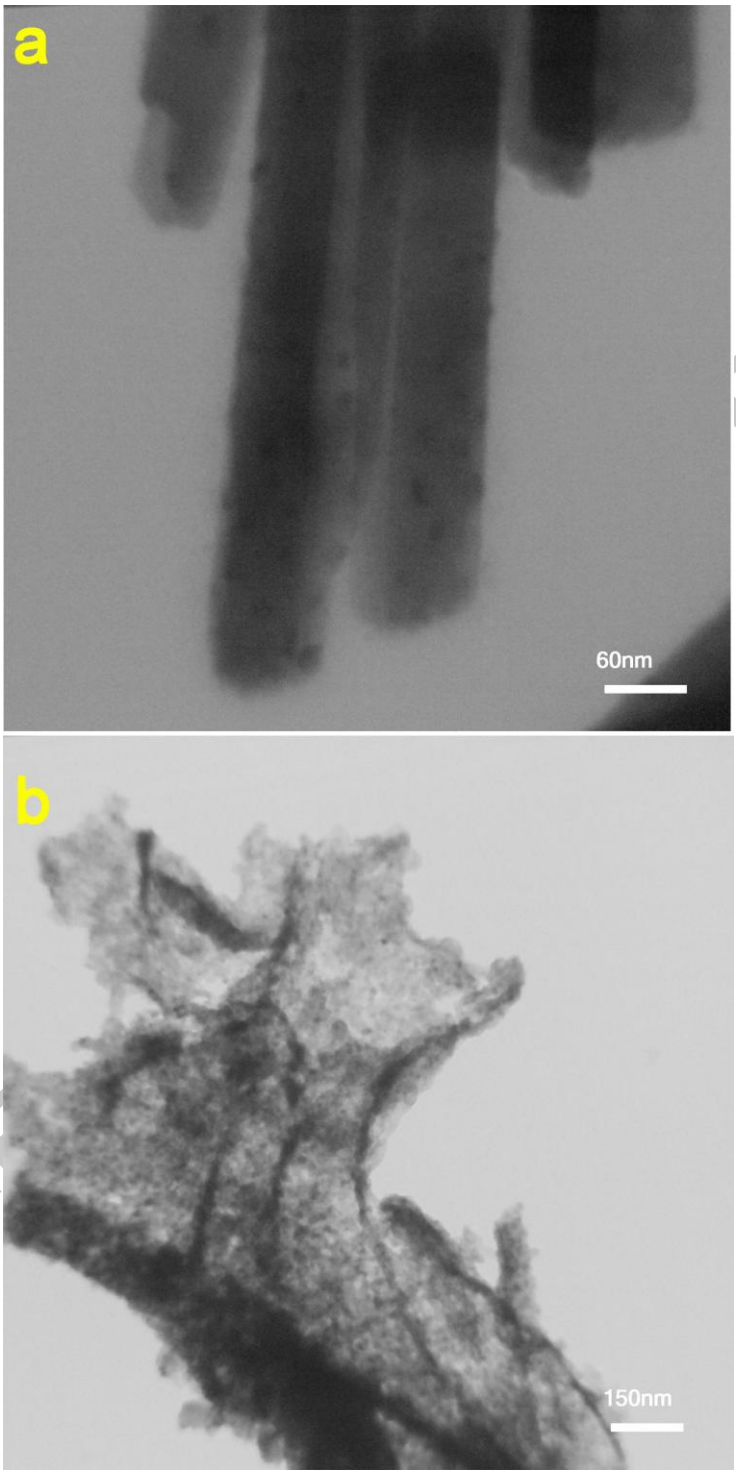

Fig.5.

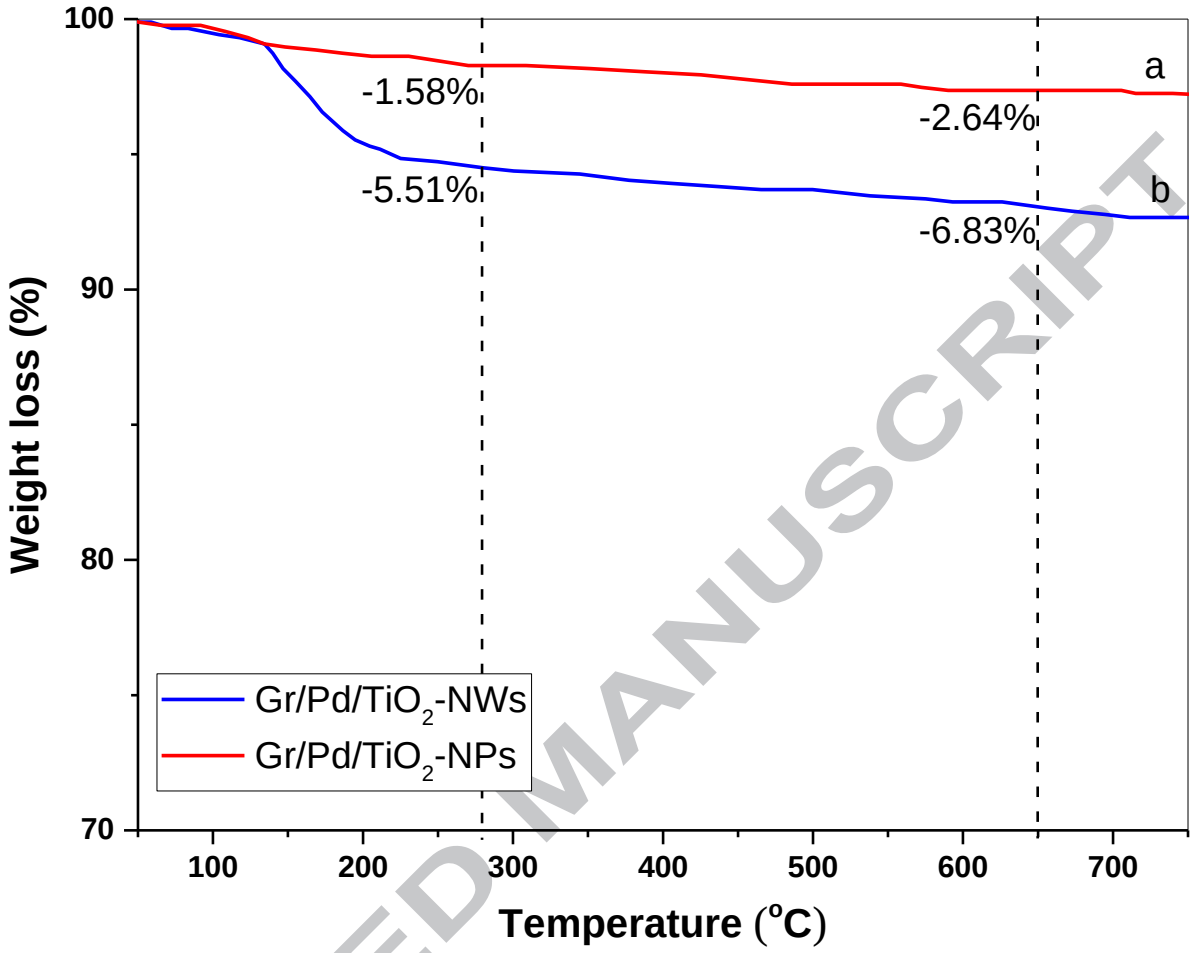

Fig.6.

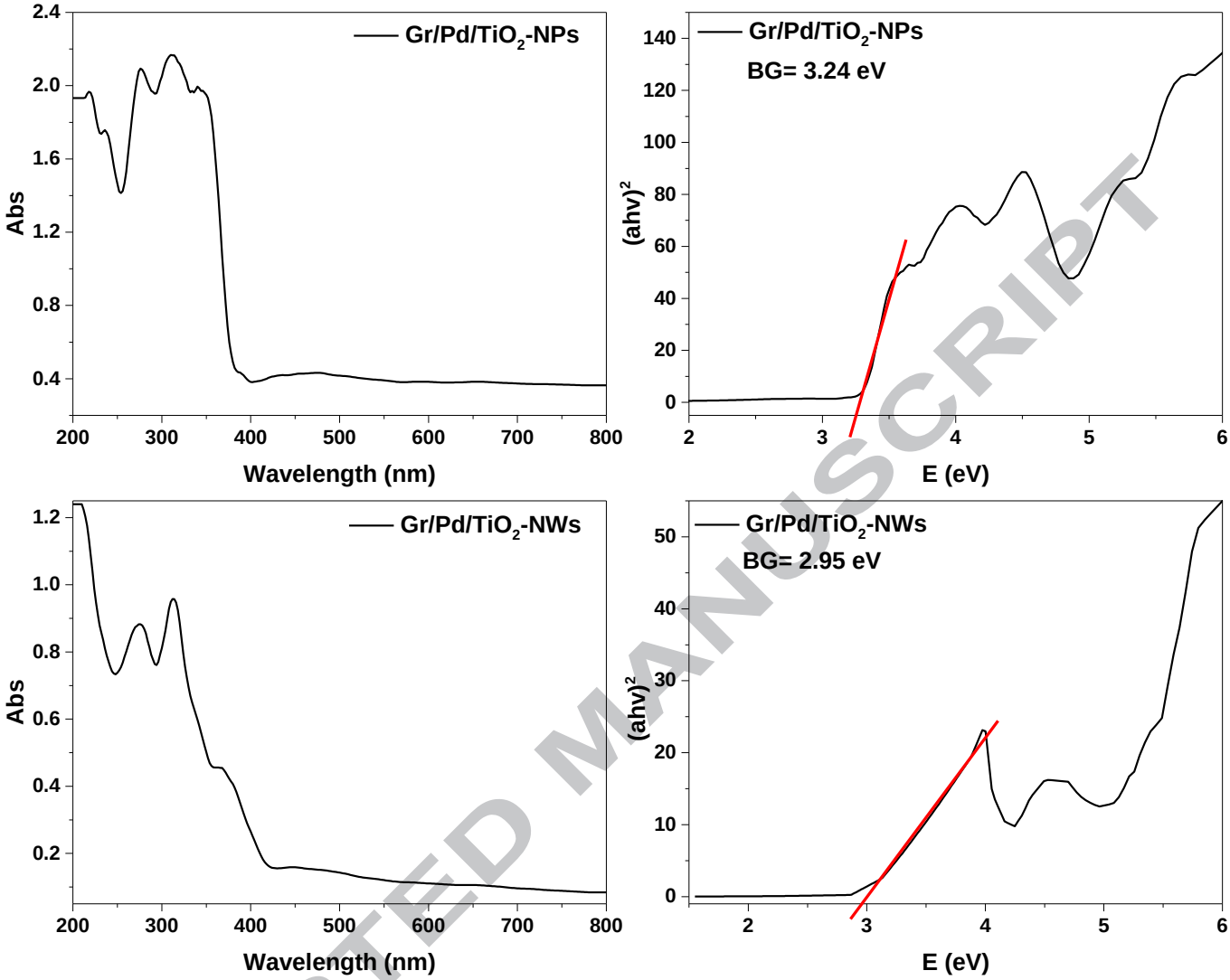

Fig.7.

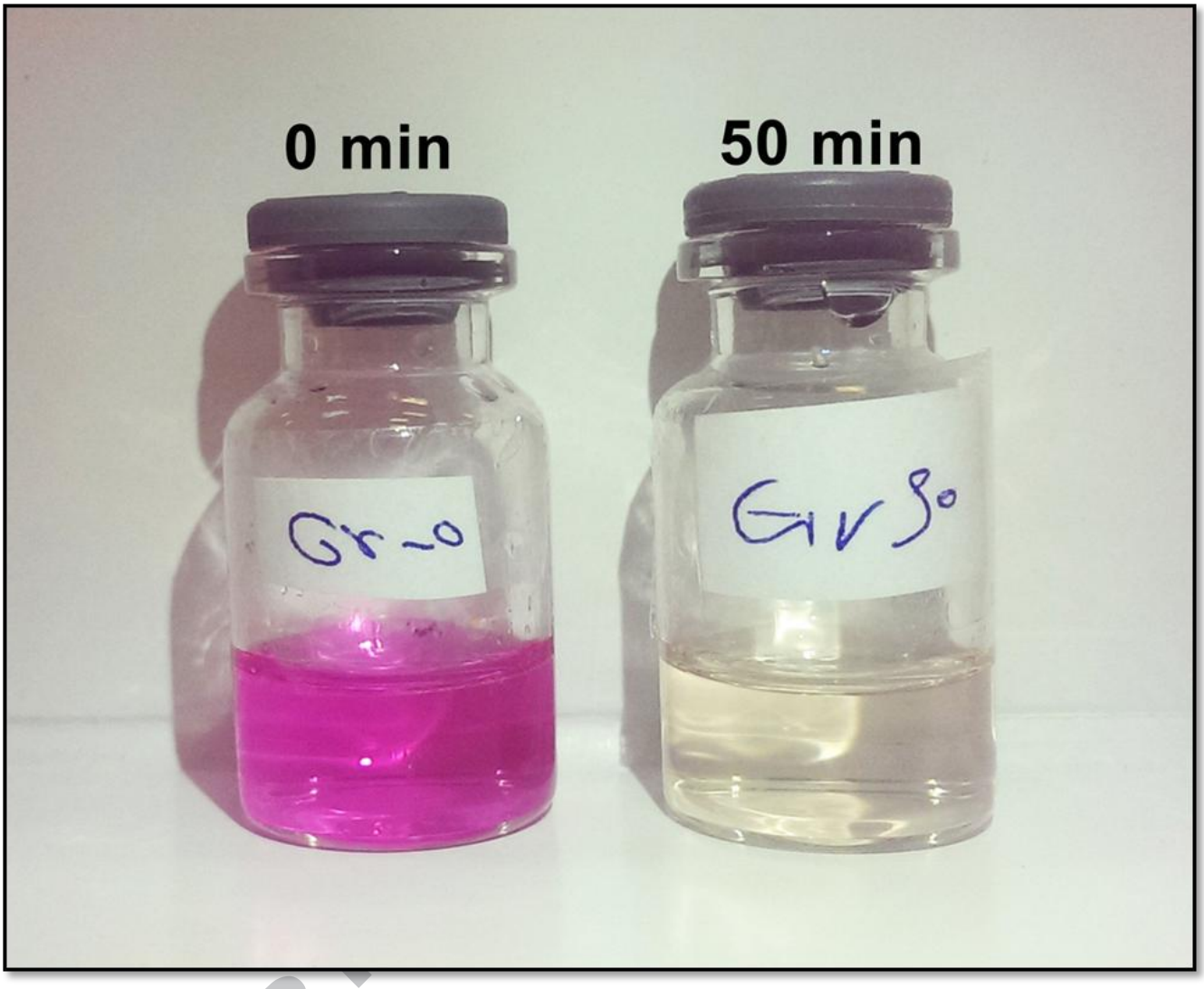

Fig.8.

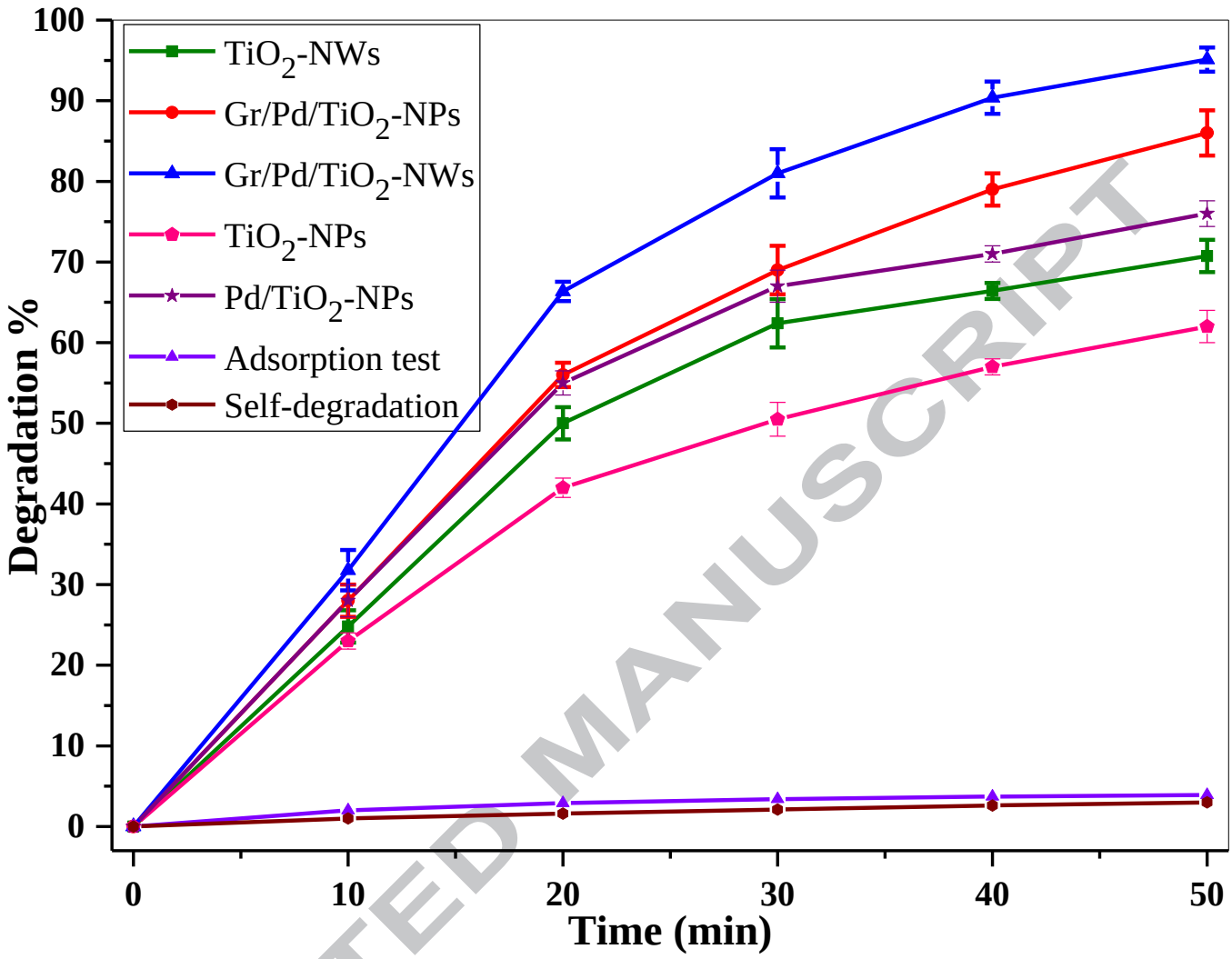

Fig.9.

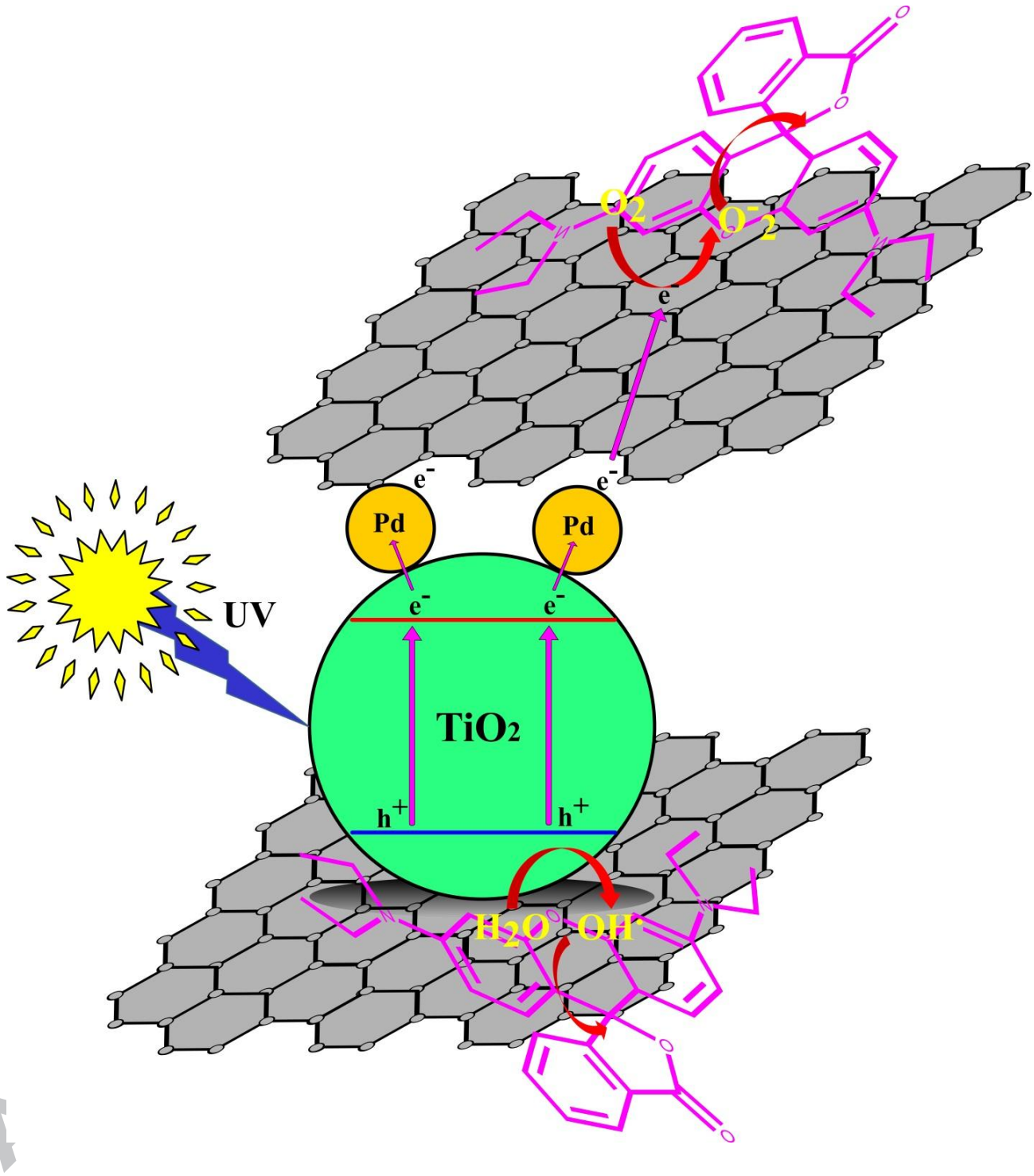

Fig.10.

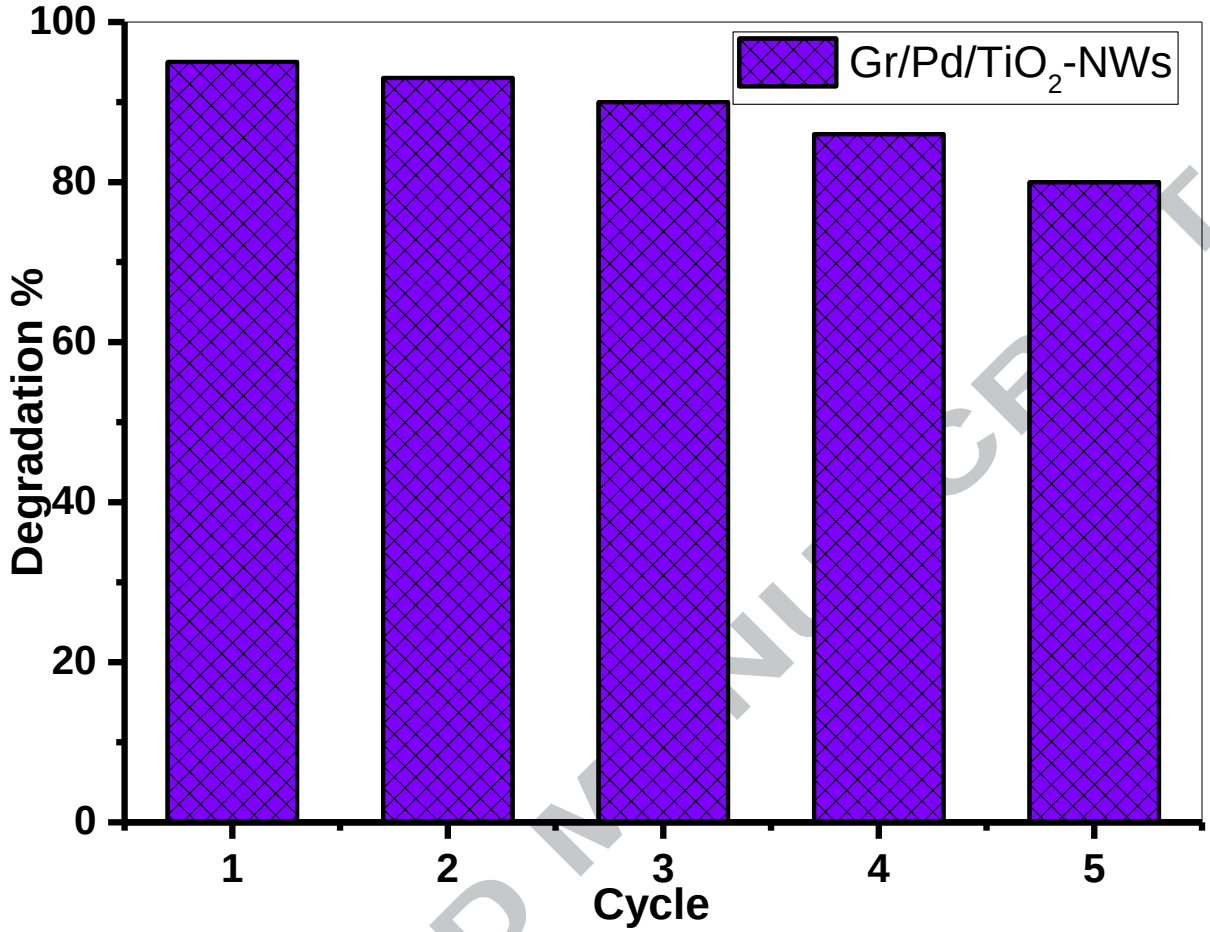

Fig.11.

Graphical abstract